An efficient numerical algorithm for computing the positive dense spectrum of the transmission eigenvalue problem with complex media

Tiexiang Li[a], Tsung-Ming Huang[b], Wen-Wei Lin[c], Jenn-Nan Wang[1]

[a]*Department of Mathematics, Southeast University, Nanjing 210096, People's Republic of China. E-mail:* `txli@seu.edu.cn`.
[b]*Department of Mathematics, National Taiwan Normal University, Taipei 116, Taiwan. E-mail:* `min@ntnu.edu.tw`.
[c]*Department of Applied Mathematics, National Chiao Tung University, Hsinchu 300, Taiwan. E-mail:* `wwlin@math.nctu.edu.tw`.
[d]*Institute of Applied Mathematics, National Taiwan University, Taipei, 106, Taiwan. E-mail:* `jnwang@math.ntu.edu.tw`.

Abstract

We study a robust and efficient eigensolver for computing the positive dense spectrum of the two-dimensional transmission eigenvalue problem (TEP) which is derived from the Maxwell's equation with complex media in pseudo-chiral model and the transverse magnetic mode. The discretized governing equations by the Nédélec edge element result in a large-scale quadratic eigenvalue problem (QEP). We estimate half of the positive eigenvalues of the QEP are on some interval which forms a dense spectrum of the QEP. The quadratic Jacobi-Davidson method with a so-called non-equivalence deflation technique is proposed to compute the dense spectrum of the QEP. Intensive numerical experiments show that our proposed method makes the convergence efficiently and robustly even it needs to compute more than 5000 desired eigenpairs. Numerical results also illustrate that the computed eigenvalue curves can be approximated by the nonlinear functions which can be applied to estimate the density of the eigenvalues for the TEP.

Keywords: Two-dimensional transmission eigenvalue problem, pseudo-chiral model, transverse magnetic mode, dense spectrum, quadratic Jacobi-Davidson method, non-equivalence deflation

1. Introduction

Transmission eigenvalue problems (TEPs) have recently received a great attention in the area of the inverse scattering which is essential for the study of direct/inverse scattering problems with nonabsorbing inhomogeneous media [1, 2, 3, 4, 8, 10, 11, 20, 26]. Transmission eigenvalues are related to the validity of some recently developed reconstruction methods for scattering problems. For instance, the linear sampling method (LSM) [5, 6] is used to reconstruct or detect the sound-soft and penetrable obstacles. The Herglotz wave function [9] is applied at the first Dirichlet eigenvalue to reconstruct the shape of scatters. The eigenvalue method using multiple frequency near-field data (EM^{2}F) [30] is proposed to detect Dirichlet or transmission eigenvalues and builds indicator functions to reconstruct the support of the target. Furthermore, the EM^{2}F can also be used to distinguish between the sound-soft obstacle and nonabsorbing inhomogeneous medium. For further study in the theories and applications of TEPs, we refer to [4] and the reference therein.

Scattering by a sound-soft or a inhomogeneous medium can be described by the near-field operator with the reciprocal gap method [7, 24]. Excluding the Dirichlet or transmission eigenvalues, the near-field operator maps a convergent sequence and a divergent sequence to the fundamental solution of the Helmholtz equation at each point inside and outside the target domain, respectively. Based on the large contrast for the near-field operator at the point inside or outside the target domain, the EM^{2}F [30] proposes an efficient eigenvalue indicator to reconstruct the support of the target object.

In fact, the near-field operator theory [7, 24] is applicable and effective only at the values which are not transmission eigenvalues of systems, i.e., not the frequency of the incident wave. This motivates us if we can change the inhomogeneous medium for the TEP so that the TEP has a dense spectrum of the positive eigenvalues. As it has shown in [3], if the refraction index of the TEP is sufficiently large, then all eigenvalues are positive and half of them are clustering in an interval near origin. This could possibly make the target object of the TEP invisible.

In this paper, we consider the scattering of accustic waves by a bounded and simply connected inhomogeneous medium domain $D \subseteq \mathbb{R}^2$. The related so-called TEP is to find $\lambda > 0$ and nontrivial functions $u, v \in L^2(D)$ with $u - v \in H_0^2(D) = \{ w \in H^2 \big| \, w = 0, \frac{\partial w}{\partial \nu} = 0 \text{ on } \partial D\}$ satisfying

$$\Delta u + \lambda \varepsilon(x, y) u = 0, \quad \text{in } D, \tag{1a}$$

$$\Delta v + \lambda v = 0, \quad \text{in } D, \tag{1b}$$

$$u - v = 0, \quad \text{on } \partial D, \tag{1c}$$

$$\frac{\partial u}{\partial \nu} - \frac{\partial v}{\partial \nu} = 0, \quad \text{on } \partial D, \tag{1d}$$

where ν is the outer unit normal to the smooth boundary ∂D and $\varepsilon(x, y)$ is the sum of refraction index plus the square of some complex media (see Sec. 2 later). Any positive λ such that (1) has nontrivial solutions u and v is called a transmission eigenvalue.

Recently, many papers have been addressed in numerical algorithms for the computation of transmission eigenvalues [3, 10, 12, 18, 19, 21, 22, 25, 26, 29, 31]. Three finite element methods (FEMs) and a coupled boundary element method were proposed for solving the two-dimensional (2D)/three-dimensional (3D) interior transmission eigenvalue problems [10, 12, 31]. Then, two iterative methods together with convergent analysis based on the existence theory of the fourth order reformulation for the transmission eigenvalues [3, 26, 29]. A mixed

FEM for 2D TEP was suggested in [18] and the corresponding non-Hermitian quadratic eigenvalue problem (QEP) was solved by the classical secant iteration with an adaptive Arnoldi method. The multilevel correction method was used to transform the solution of TEP into a series of solutions corresponding to linear boundary value problems and then solved by the multigrid method [19].

In many cases with general inhomogeneous medium, the desired positive TEP are surrounded by complex eigenvalues. An accurate numerical method, based on a surface integral formulation of the interior TEP, for solving corresponding nonlinear eigenvalue problems for many different obstacles in 3D is presented in [21]. However, only constant index of refraction and smooth domain can be treated. The QEPs above can be rewritten as a particular parametrized symmetric definite GEPs for which the eigenvalue curves are arranged in a monotonic order so that the desired curves can be sequentially solved with a new secant-type iteration (see [22] for 2D TEP and [13] for 3D TEP, respectively).

In this paper, we focus on the 2D TEP with complex media and make the following contributions.

- We derive the 2D TEP (1) with $\varepsilon(x, y) = n(x, y) + \gamma^2$ from the Maxwell's equation with complex media in pseudo-chiral model and the transverse magnetic mode (TM). Here $n(x, y)$ is the index of refraction and $\gamma > 0$ is a chirality parameter.

- Discretized (1) by the Nédélec edge element [10] results in a generalized eigenvalue problem (GEP). The GEP is then reduced to a QEP by deflating all nonphysical zeros. We estimate half of the positive eigenvalues of the QEP are on some interval which forms a dense spectrum of the QEP.

- We adapt the quadratic Jacobi-Davidson (QJD) method with partial locking technique for computing a large number of desired eigenpairs of the QEP. In order to accelerate convergence, we also develop a so-called partial non-equivalence deflation technique combined with QJD to deflate the part of computed eigenvalues to infinity while keeping the other eigenvalues unchanged. Numerical results demonstrate that the new partial deflation technique makes the convergence efficiently and robustly for computing 5000 desired eigenpairs.

- Furthermore, we modify QJD with partial deflation technique so that it can be applied to compute all the eigenvalues in a given interval. Therefore, we separate the dense spectrum of the TEP into serval subintervals and compute the desired eigenpairs simultaneously by the modified method. Numerical results show that this modified method can be applied to compute more than 10000 target eigenpairs in our model.

- According to the computed eigenvalues, we make some approximations of the eigenvalue curves for the TEP (1) by the nonlinear functions. Therefore, we can estimate the distribution of the eigenvalues for given $\varepsilon(x, y)$ from these nonlinear functions.

This paper is organized as follows. Section 2 is devoted to derive a 2D TEP with TM mode and complex media in pseudo-chiral model. A corresponding discretization TEP and its spectral analysis are given in Section 3. In Section 4, we develop a non-equivalence low-rank deflation which can be used to accelerate convergence of QJD for computing the desired positive eigenvalues. A practical QJD algorithm combined with non-equivalence deflation and numerical results are presented in Sections 5 and 6, respectively. Finally, a concluding remark is given in Section 7.

2. Maxwell's transmission eigenvalue problem with complex media and TM mode

Mathematically, the propagation of electromagnetic waves in bi-isotropic and bi-anisotropic material is modeled by the 3D frequency domain source-free Maxwell equations. In this paper, we consider a 2D Maxwell's equation with TM mode and complex media in pseudo-chiral model [32]

$$\nabla \times E = \mathrm{i}\omega \left(\mu H + \zeta E\right), \tag{2a}$$
$$\nabla \times H = -\mathrm{i}\omega \left(n E + \xi H\right), \tag{2b}$$

where E and H are the electronic field and magnetic field, respectively, ω represents the frequency, n and μ are the permittivity/refraction index and permeability, respectively, ξ and ζ are 3-by-3 magnetoelectric parameter matrices in various forms for describing different types of materials (see [27, p.26] and [32, p.44]). In particular, we consider E and H in (2) forming the transversal magnetic (TM) mode, i.e.,

$$E = \begin{bmatrix} 0 & 0 & E_3(x,y) \end{bmatrix}^\top, \quad H = \begin{bmatrix} H_1(x,y) & H_2(x,y) & 0 \end{bmatrix}^\top. \tag{3}$$

Let

$$\zeta = \begin{bmatrix} 0 & 0 & \zeta_1 \\ 0 & 0 & \zeta_2 \\ -\zeta_1 & -\zeta_2 & 0 \end{bmatrix}, \quad \xi = \begin{bmatrix} 0 & 0 & \xi_1 \\ 0 & 0 & \xi_2 \\ -\xi_1 & -\xi_2 & 0 \end{bmatrix}. \tag{4}$$

Then, Eqs. (2a) implies that

$$\begin{bmatrix} \partial_y E_3 \\ -\partial_x E_3 \\ 0 \end{bmatrix} = \mathrm{i}\omega \left(\begin{bmatrix} H_1 \\ H_2 \\ 0 \end{bmatrix} + \begin{bmatrix} \zeta_1 E_3 \\ \zeta_2 E_3 \\ 0 \end{bmatrix} \right). \tag{5}$$

Substituting (5) into (2b), it holds that

$$\begin{aligned} &(\mathrm{i}\omega)^{-1} \begin{bmatrix} 0 \\ 0 \\ -\left(\frac{\partial^2}{\partial x^2} + \frac{\partial^2}{\partial y^2}\right) E_3 \end{bmatrix} - \begin{bmatrix} 0 \\ 0 \\ \frac{\partial}{\partial x}\left(\zeta_2 E_3\right) - \frac{\partial}{\partial y}\left(\zeta_1 E_3\right) \end{bmatrix} \\ = &-\mathrm{i}\omega \left(n \begin{bmatrix} 0 \\ 0 \\ E_3 \end{bmatrix} + \begin{bmatrix} 0 \\ 0 \\ \xi_1 H_1 + \xi_2 H_2 \end{bmatrix} \right), \end{aligned}$$

which implies that

$$
\begin{aligned}
&-\Delta E_3\\
&=\omega^2\left[nE_3+\xi_1\left((\mathrm{i}\omega)^{-1}\frac{\partial}{\partial y}E_3-\zeta_1E_3\right)-\xi_2\left((\mathrm{i}\omega)^{-1}\frac{\partial}{\partial x}E_3+\zeta_2E_3\right)\right]\\
&\quad+\mathrm{i}\omega\left[\frac{\partial}{\partial x}\left(\zeta_2E_3\right)-\frac{\partial}{\partial y}\left(\zeta_1E_3\right)\right]\\
&=\omega^2\left(n-\xi_1\zeta_1-\xi_2\zeta_2\right)E_3+\mathrm{i}\omega\left[\frac{\partial}{\partial x}\left(\zeta_2E_3\right)-\frac{\partial}{\partial y}\left(\zeta_1E_3\right)-\xi_1\frac{\partial}{\partial y}E_3+\xi_2\frac{\partial}{\partial x}E_3\right].
\end{aligned}
$$

If we choose $\zeta_1=-\xi_1=\gamma_1$ and $\zeta_2=-\xi_2=\gamma_2$, then we have

$$
-\Delta E_3=\omega^2\left[n+\left(\gamma_1^2+\gamma_2^2\right)\right]E_3\equiv\omega^2\varepsilon(x,y)E_3. \tag{6}
$$

For satisfying the boundary conditions with ν being the outer unit normal to ∂D, we have

$$
E\times\nu=\begin{bmatrix}0\\0\\E_3\end{bmatrix}\times\begin{bmatrix}\nu_1\\\nu_2\\0\end{bmatrix}=\begin{bmatrix}-\nu_2E_3\\\nu_1E_3\\0\end{bmatrix} \tag{7}
$$

and

$$
(\nabla\times E)\times\nu=\begin{bmatrix}\frac{\partial}{\partial y}E_3\\-\frac{\partial}{\partial x}E_3\\0\end{bmatrix}\times\begin{bmatrix}\nu_1\\\nu_2\\0\end{bmatrix}=\begin{bmatrix}\frac{\partial E_3}{\partial y}\nu_2+\frac{\partial E_3}{\partial x}\nu_1\\0\\0\end{bmatrix}=\begin{bmatrix}\frac{\partial E_3}{\partial\nu}\\0\\0\end{bmatrix}. \tag{8}
$$

Let v^i be the incident plane wave in $\mathbb{R}^2$, u be the transmitted plane wave in D, v^s be the scattered plane wave in $\mathbb{R}^2\backslash D$ and $\tilde{v}^s$ be the analytic extension of v^s in D. Then $u=E_3$ satisfies the Eq. (6) and $v=v^i+\tilde{v}^s$ satisfies the Helmholtz equation $\Delta v+\omega^2v=0$. From (7) and (8), we connect the boundary conditions of u and v by equaling $u=v$ and $\frac{\partial u}{\partial\nu}=\frac{\partial v}{\partial\nu}$ on ∂D, and get the 2D TEP (1) with $\lambda=\omega^2$.

3. Discretization of TEP and its spectral analysis

We briefly review the discretization of the TEP (1) based on the standard piecewise linear FEM (see [10] for details). Let

$S_h=$ The space of continuous piecewise linear functions on D,

$S_h^I=$ The subspace of functions in S_h that have vanishing DoF on ∂D,

$S_h^B=$ The subspace of functions in S_h that have vanishing DoF in D, where DoF is the degrees of freedom. Let $\{\phi_i\}_{i=1}^n$ and $\{\psi_i\}_{i=1}^m$ denote standard nodal bases for the finite element spaces of S_h^I and S_h^B, respectively. Then

$$u = u_h^I + u_h^B = \sum_{i=1}^n u_i\phi_i + \sum_{i=1}^m w_i\psi_i, \tag{9a}$$

$$v = v_h^I + v_h^B = \sum_{i=1}^n v_i\phi_i + \sum_{i=1}^m w_i\psi_i. \tag{9b}$$

Applying the standard piecewise linear finite element method to (1a) and using the integration by part, we get

$$\begin{aligned}&\sum_{i=1}^n u_i\left(\nabla\phi_i, \nabla\phi_j\right) + \sum_{j=1}^m w_i\left(\nabla\psi_i, \nabla\phi_j\right)\\ &= \omega^2\left(\sum_{i=1}^n u_i\left(\varepsilon\phi_i, \phi_j\right) + \sum_{i=1}^m w_i\left(\varepsilon\psi_i, \phi_j\right)\right).\end{aligned} \tag{10}$$

Similarly, applying the standard piecewise linear finite element method to (1b), we have

$$\sum_{i=1}^n v_i\left(\nabla\phi_i, \nabla\phi_j\right) + \sum_{j=1}^m w_i\left(\nabla\psi_i, \nabla\phi_j\right) = \omega^2\left(\sum_{i=1}^n v_i\left(\phi_i, \phi_j\right) + \sum_{i=1}^m w_i\left(\psi_i, \phi_j\right)\right). \tag{11}$$

Applying the linear finite element method with boundary conditions (1c), (1d) and the integration by part to the difference equation between (1a) and (1b), we get

$$\begin{aligned}&\left(\sum_{i=1}^n (u_i - v_i)\nabla\phi_i, \nabla\psi_j\right)\\ &= \omega^2\left(\sum_{i=1}^n u_i(\varepsilon\phi_i, \psi_j) + \sum_{i=1}^m w_i(\varepsilon\phi_i, \psi_j) - \sum_{i=1}^n v_i(\phi_i, \psi_j) - \sum_{i=1}^m w_i(\phi_i, \psi_j)\right).\end{aligned} \tag{12}$$

We define the stiffness matrices K, E, and mass matrices M_1, M_ε, F_1, F_ε, G_1 and G_ε as in Table 1. In addition, we set $\mathbf{u} = [u_1, \ldots, u_n]^\top$, $\mathbf{v} = [v_1, \ldots, v_n]^\top$, and $\mathbf{w} = [w_1, \ldots, w_m]^\top$. Then, the discretizations of (10), (11) and (12) give rise to a generalized eigenvalue problem (GEP)

$$\mathcal{A}\mathbf{z} = \lambda\mathcal{B}\mathbf{z} \tag{13a}$$

with $\lambda = \omega^2$,

$$\mathcal{A} = \begin{bmatrix} K & 0 & E \\ 0 & -K & E \\ E^\top & E^\top & 0 \end{bmatrix},\ \mathcal{B} = \begin{bmatrix} M_\varepsilon & 0 & F_\varepsilon \\ 0 & -M_1 & F_1 \\ F_\varepsilon^\top & F_1^\top & G_\varepsilon - G_1 \end{bmatrix},\ \mathbf{z} = \begin{bmatrix} \mathbf{u} \\ \mathbf{v} \\ \mathbf{w} \end{bmatrix}. \tag{13b}$$

Matrix	Dimension	Definition
$K \succ 0$	$n \times n$	interior space stiffness matrix: $K_{ij} = (\nabla\phi_i, \nabla\phi_j)$
E	$n \times m$	interior/boundary stiffness matrix: $E_{ij} = (\nabla\phi_i, \nabla\psi_j)$
$M_1 \succ 0, M_\varepsilon \succ 0$	$n \times n$	interior space mass matrices: $(M_1)_{ij} = (\phi_i, \phi_j)$, $(M_\varepsilon)_{ij} = (\varepsilon\phi_i, \phi_j)$
F_1, F_ε	$n \times m$	interior/boundary mass matrices: $(F_1)_{ij} = (\phi_i, \psi_j)$, $(F_\varepsilon)_{ij} = (\varepsilon\phi_i, \psi_j)$
$G_1 \succ 0, G_\varepsilon \succ 0$	$m \times m$	boundary space mass matrices: $(G_1)_{ij} = (\psi_i, \psi_j)$, $(G_\varepsilon)_{ij} = (\varepsilon\psi_i, \psi_j)$

Table 1: Stiffness and mass matrices with $\varepsilon(x, y) > 0$ for $(x, y) \in \bar{D}$.

For the convenience, we define

$$G = G_\varepsilon - G_1, \quad M = M_\varepsilon - M_1, \quad F = F_\varepsilon - F_1, \tag{14a}$$

$$\widehat{M}_1 = M_1 - F_1 G^{-1} F^\top, \quad \widehat{M} = M - F G^{-1} F^\top, \quad \widehat{K} = K - E G^{-1} F^\top, \tag{14b}$$

and

$$\mathcal{S} = \begin{bmatrix} K & E \end{bmatrix}, \quad \mathcal{T}_1 = \begin{bmatrix} M_1 & F_1 \end{bmatrix}, \quad \mathcal{M} = \begin{bmatrix} M & F \\ F^\top & G \end{bmatrix}. \tag{14c}$$

Suppose that $\mathcal{M} \succ 0$ symmetric positive definite. Then it follows that $G \succ 0$, $M \succ 0$ and $\widehat{M} \succ 0$.

We define the quadratic eigenvalue problem (QEP)

$$\mathcal{Q}(\lambda)\mathbf{x} \equiv \left(\lambda^2 A_2 + \lambda A_1 + A_0\right)\mathbf{x} = 0, \tag{15}$$

where A_2, A_1 and A_0 are all $n \times n$ symmetric matrices given by

$$\begin{aligned} A_2 &= M_1 + \widehat{M}_1 \widehat{M}^{-1} \widehat{M}_1^\top + F_1 G^{-1} F_1^\top && (16a) \\ &= M_1 + \mathcal{T}_1 \mathcal{M}^{-1} \mathcal{T}_1^\top, \\ A_1 &= -K - \widehat{K} \widehat{M}^{-1} \widehat{M}_1^\top - \widehat{M}_1 \widehat{M}^{-1} \widehat{K}^\top - E G^{-1} F_1^\top - F_1 G^{-1} E^\top && (16b) \\ &= -K - \mathcal{S} \mathcal{M}^{-1} \mathcal{T}_1^\top - \mathcal{T}_1 \mathcal{M}^{-1} \mathcal{S}^\top, \\ A_0 &= \widehat{K} \widehat{M}^{-1} \widehat{K}^\top + E G^{-1} E^\top && (16c) \\ &= \mathcal{S} \mathcal{M}^{-1} \mathcal{S}^\top. \end{aligned}$$

It has shown [13] that the GEP (13) can be reduced to the QEP as in (15) and (16) with $\mathbf{x} = \mathbf{u} - \mathbf{v}$ in which all nonphysical zero are removed.

Theorem 1 ([13])**.** *Let $\mathcal{L}(\lambda)$ and $\mathcal{Q}(\lambda)$ be defined in* (13) *and* (15)*, respectively. Then*

$$\sigma(\mathcal{L}(\lambda)) = \underbrace{\{0, \cdots, 0\}}_{m} \cup \sigma(\mathcal{Q}(\lambda)).$$

Here, $\sigma(\cdot)$ denotes the spectrum of the associated matrix pencil.

Let $(\lambda, \mathbf{x})$ be an eigenpair of (15). Then

$$\lambda^2(\mathbf{x}^* A_2 \mathbf{x}) + \lambda(\mathbf{x}^* A_1 \mathbf{x}) + (\mathbf{x}^* A_0 \mathbf{x}) = 0. \tag{17}$$

Suppose A_1 is symmetric negative definite and $A_2, A_0 \succ 0$, we have

$$b \equiv -\mathbf{x}^* A_1 \mathbf{x} > 0, \quad a \equiv \mathbf{x}^* A_2 \mathbf{x} > 0, \quad c \equiv \mathbf{x}^* A_0 \mathbf{x} > 0$$

which implies that the roots of the quadratic equation (17) are

$$\lambda_+ = \frac{b + \sqrt{b^2 - 4ac}}{2a} > 0, \quad \lambda_- = \frac{2c}{b + \sqrt{b^2 - 4ac}} > 0 \tag{18}$$

provided that $b^2 - 4ac > 0$. This means that there are $2n$ positive eigenvalues of (15) and the associated eigenvectors are real.

Theorem 2. *Let*

$$W_0 = \begin{bmatrix} M & F \\ F^\top & G \end{bmatrix}^{-1/2} \begin{bmatrix} K \\ E^\top \end{bmatrix}, \quad W_1 = \begin{bmatrix} M & F \\ F^\top & G \end{bmatrix}^{-1/2} \begin{bmatrix} M_1 \\ F_1^\top \end{bmatrix}, \tag{19}$$

$$d_0 = \|W_0\|_2, \quad d_1 = \|W_1\|_2, \tag{20}$$

and

$$\begin{cases} \underline{a}_0 = \lambda_{\min}(A_0), & \bar{a}_0 = \lambda_{\max}(A_0) = d_0^2, \\ \underline{a}_2 = \lambda_{\min}(A_2), & \bar{a}_2 = \lambda_{\max}(A_2). \end{cases} \tag{21}$$

Suppose that

$$\underline{a}_1 = \lambda_{\min}(K) - 2d_0 d_1 > 0, \quad \bar{a}_1 = \lambda_{\max}(K) + 2d_0 d_1, \tag{22}$$

$$\delta = \lambda_{\min}(K)^2 - 4d_0(d_1 \lambda_{\min}(K) + d_0 \lambda_{\max}(M_1)) > 0. \tag{23}$$

Then there are n positive eigenvalues of (15) in the interval (r_*, r^*), where

$$r^* = \frac{2d_0^2}{\underline{a}_1 + \sqrt{\delta}}, \quad r_* = \frac{2\lambda_{\min}(A_0)}{\bar{a}_1 + \sqrt{\bar{a}_1 - 4\underline{a}_2\underline{a}_0}} > 0. \tag{24}$$

Proof. By the definitions of W_0 and W_1, A_1 in (16b) can be represented as

$$A_1 = -(K + W_0^\top W_1 + W_1^\top W_0). \tag{25}$$

Let $\mathbf{x}$ be the unit eigenvector of (15). Eq. (25) tells us that

$$\begin{aligned} b &\equiv -\mathbf{x}^\top A_1 \mathbf{x} = \mathbf{x}^\top K \mathbf{x} + \mathbf{x}^\top W_0^\top W_1 \mathbf{x} + \mathbf{x}^\top W_1^\top W_0 \mathbf{x} \\ &\geq \lambda_{\min}(K) - 2d_0 d_1 = \underline{a}_1 > 0. \end{aligned}$$

Let $a = \mathbf{x}^\top A_2\mathbf{x}$ and $c = \mathbf{x}^\top A_0\mathbf{x}$. Then

$$\begin{aligned} b^2 - 4ac &\geq (\lambda_{\min}(K) - 2d_0d_1)^2 - 4d_0^2(\lambda_{\min}(M_1) + d_1^2) \\ &= \lambda_{\min}(K)^2 - 4d_0(d_1\lambda_{\min}(K) + d_0\lambda_{\max}(M_1)) = \delta > 0. \end{aligned}$$

Therefore,

$$\lambda_- = \frac{2c}{b + \sqrt{b^2 - 4ac}} \leq \frac{2d_0^2}{\underline{a}_1 + \sqrt{\delta}} = r^*.$$

On the other hand,

$$\begin{aligned} b = -\mathbf{x}^\top A_1\mathbf{x} \leq \lambda_{\max}(K) + 2d_0d_1 = \bar{a}_1, \\ b^2 - 4ac \leq \bar{a}_1^2 - 4\underline{a}_2\underline{a}_0. \end{aligned}$$

Therefore,

$$\lambda_- = \frac{2c}{b + \sqrt{b^2 - 4ac}} \geq \frac{2\underline{a}_0}{\bar{a}_1 + \sqrt{\bar{a}_1^2 - 4\underline{a}_2\underline{a}_0}} = r_*.$$

From (18), there are n smallest positive eigenvalues on (r_*, r^*). □

Remark 3. *From* (16c)*, the value* $\mathbf{x}^\top A_0\mathbf{x}$ *is dominated by* $\mathbf{x}^\top \widehat{K}\widehat{M}^{-1}\widehat{K}^\top\mathbf{x}$ *provided that* $\lambda_{\min}(K) = O(\kappa) \gg 1$*. From* (16a)*, it holds that* $\mathbf{x}^\top A_2\mathbf{x} \approx O(1)$*. If we can choose the coefficient* $\varepsilon(x, y)$ *in* (1a) *such that* $M \approx K$*, then from* (24) *follows that*

$$\lambda_- \approx \frac{2O(\kappa)}{O(\kappa) + \sqrt{O(\kappa)^2 + O(\kappa)}} \approx O(1).$$

It means that there are n *positive eigenvalues of* (1) *which may form a dense spectrum in the interval* $(0, O(1))$*. This motivates us to develop efficient numerical algorithms to compute all smallest clustering positive eigenvalues.*

4. Non-equivalence low-rank deflation

In this section, we introduce the non-equivalence low-rank deflation [14] for the QEP in (15) to find the successive eigenpairs. Once the smallest positive eigenvalue is obtained, it is then transformed to infinity by the deflation scheme, while all other eigenvalues remain unchanged. The next successive eigenvalue thus becomes the target positive eigenvalue of the transformed problem, which is then again solved by the proposed method.

Definition 4 ([14])**.** *Let* $(\Lambda_1, X_1) \in \mathbb{R}^{r\times r} \times \mathbb{R}^{n\times r}$ *be a given pair, where* X_1 *is of full column rank. The pair* (Λ_1, X_1) *is called an eigenmatrix pair of* $\mathcal{Q}(\lambda)$ *in* (15) *if it satisfies*

$$A_2X_1\Lambda_1^2 + A_1X_1\Lambda_1 + A_0X_1 = 0. \tag{26}$$

In particular, $(\mathrm{diag}(\infty, \cdots, \infty), X_1)$ *is called an "infinity" eigenmatrix pair of* $\mathcal{Q}(\lambda)$ *if* $A_2X_1 = 0$*.*

Given an eigenmatrix pair $(\Lambda_1, X_1) \in \mathbb{R}^{r\times r} \times \mathbb{R}^{n\times r}(r \le n)$ of $\mathcal{Q}(\lambda)$ in (15), where Λ_1 is nonsingular, we define a new deflated QEP as

$$\mathcal{Q}_d(\lambda) := \lambda^2 \widetilde{A}_2 + \lambda \widetilde{A}_1 + \widetilde{A}_0 \tag{27}$$

with

$$\widetilde{A}_2 := A_2 - A_2 X_1 \Theta_1 X_1^\top A_2, \tag{28a}$$

$$\widetilde{A}_1 := A_1 + A_2 X_1 \Theta_1 \Lambda_1^{-\top} X_1^\top A_0 + A_0 X_1 \Lambda_1^{-1} \Theta_1 X_1^\top A_2, \tag{28b}$$

$$\widetilde{A}_0 := A_0 - A_0 X_1 \Lambda_1^{-1} \Theta_1 \Lambda_1^{-\top} X_1^\top A_0 \tag{28c}$$

and

$$\Theta_1 := (X_1^\top A_2 X_1)^{-1}. \tag{28d}$$

The nonequivalence deflation (28) allows us to transform $\mathcal{Q}(\lambda)$ into a new QEP $\mathcal{Q}_d(\lambda)$ with the same eigenvalues, except that the eigenvalues of Λ_1 are replaced by r infinities.

On the other hand, let $(\Lambda_2, X_2) \in \mathbb{R}^{s\times s} \times \mathbb{R}^{n\times s}$ be another eigenmatrix pair of $\mathcal{Q}(\lambda)$. Suppose that $\sigma(\Lambda_1) \cap \sigma(\Lambda_2) = \emptyset$. Then the following orthogonality relation holds

$$X_2^\top A_0 X_1 - \Lambda_2^\top (X_2^\top A_2 X_1) \Lambda_1 = 0. \tag{29}$$

Using this orthogonality relation, we can get that (Λ_2, X_2) is also an eigenmatrix pair of $\mathcal{Q}_d(\lambda)$.

5. Jacobi-Davidson method for quadratic eigenvalue problems

In this section, we propose the quadratic Jacobi-Davidson (QJD) method [15, 28] with the non-equivalence deflating scheme to solve the QEP (15). Suppose $\mathcal{V}_k$ is a k-dimensional subspace that has an orthogonal unitary basis $\mathbf{v}_1, \mathbf{v}_2, \ldots, \mathbf{v}_k$. Let $(\theta_k, \mathbf{s}_k)$ be an eigenpair of $V_k^* \mathcal{Q}(\lambda) V_k \mathbf{s} = 0$ and $(\theta_k, \mathbf{u}_k \equiv V_k \mathbf{s}_k)$ be a Ritz pair of $\mathcal{Q}(\lambda)$, where $\|\mathbf{s}_k\|_2 = 1$ and $V_k = [\mathbf{v}_1, \cdots, \mathbf{v}_k]$. To expand the subspace $\mathcal{V}_k$ successively, the QJD method finds the approximated solution of the following correction equation:

$$\left(I - \frac{\mathbf{p}_k \mathbf{u}_k^*}{\mathbf{u}_k^* \mathbf{p}_k}\right) \mathcal{Q}(\theta_k) \left(I - \mathbf{u}_k \mathbf{u}_k^*\right) \mathbf{t} = -\mathbf{r}_k, \quad \mathbf{t} \perp \mathbf{u}_k, \tag{30}$$

where $\mathbf{r}_k = \mathcal{Q}(\theta_k)\mathbf{u}_k$ and $\mathbf{p}_k = (2\theta_k A_2 + A_1)\mathbf{u}_k$. This is an essential step in the QJD method that may affect the overall performance significantly.

There are different schemes [15] to solve (30). In here, based on the coefficient matrices A_0, A_1, A_2 in (16), we use the following scheme proposed in [15] to solve (30). Using the constraint $\mathbf{t} \perp \mathbf{u}_k$, Eq. (30) can be rewritten as

$$\mathcal{Q}(\theta_k)\mathbf{t} = \frac{\mathbf{u}_k^* \mathcal{Q}(\theta_k)\mathbf{t}}{\mathbf{u}_k^* \mathbf{p}_k} \mathbf{p}_k - \mathbf{r}_k \equiv \eta_k \mathbf{p}_k - \mathbf{r}_k. \tag{31}$$

We can then solve the two linear systems

$$\mathcal{Q}(\theta_k)\mathbf{t}_1 = \mathbf{p}_k, \quad \mathcal{Q}(\theta_k)\mathbf{t}_2 = \mathbf{r}_k \tag{32a}$$

and compute the solution $\mathbf{t}$ of (31) as

$$\mathbf{t} = \eta_k \mathbf{t}_1 - \mathbf{t}_2 \text{ with } \eta_k = \frac{\mathbf{u}_k^* \mathbf{t}_2}{\mathbf{u}_k^* \mathbf{t}_1}. \tag{32b}$$

Based on the above discussions, a quadratic Jacobi-Davidson method designed to compute the desired eigenvalue for the QEP (15) is shown in Algorithm 1.

Algorithm 1 QJD method for $\mathcal{Q}(\lambda)\mathbf{x} \equiv (\lambda^2 A_2 + \lambda A_1 + A_0)\mathbf{x} = 0$.

Require: Coefficient matrices A_0, A_1, A_2 and an initial orthonormal vector V.
Ensure: The desired eigenpair $(\lambda, \mathbf{x})$.

1: Compute $W_i = A_i V$ and $M_i = V^* W_i$ for $i = 0, 1, 2$.
2: **while** (the desired eigenpair is not convergent) **do**
3: Compute the eigenpairs $(\theta, \mathbf{s})$ of $(\theta^2 M_2 + \theta M_1 + M_0)\mathbf{s} = 0$.
4: Select the desired eigenpair $(\theta, \mathbf{s})$ with $\|\mathbf{s}\|_2 = 1$.
5: Compute $\mathbf{u} = V\mathbf{s}$, $\mathbf{p} = (2\theta A_2 + A_1)\mathbf{u}$, $\mathbf{r} = \mathcal{Q}(\theta)\mathbf{u}$.
6: Solve the correction vector $\mathbf{t}$ in (32).
7: Orthogonalize $\mathbf{t}$ against V; set $\mathbf{v} = \mathbf{t}/\|\mathbf{t}\|_2$.
8: Compute

$$\mathbf{w}_i = A_i \mathbf{v}, \quad M_i = \begin{bmatrix} M_i & V^* \mathbf{w}_i \\ \mathbf{v}^* W_i & \mathbf{v}^* \mathbf{w}_i \end{bmatrix}$$

for $i = 0, 1, 2$.
9: Expand $V = [V, \mathbf{v}]$ and $W_i = [W_i, \mathbf{w}_i]$ for $i = 0, 1, 2$.
10: **end while**
11: Set $\lambda = \theta$ and $\mathbf{x} = \mathbf{u}$.

Note that the solutions $\mathbf{t}_1$ and $\mathbf{t}_2$ in (32a) can be efficiently computed by following way. Substituting A_2, A_1 and A_0 in (16) into (32a), Eq. (32a) can be represented as

$$\begin{aligned} \Big\{ \theta_k^2 M_1 - \theta_k K + \left(\theta_k \widehat{M}_1 - \widehat{K}\right) \widehat{M}^{-1} \left(\theta_k \widehat{M}_1^\top - \widehat{K}^\top\right) \\ + \left(\theta_k F_1 - E\right) G^{-1} \left(\theta_k F_1^\top - E^\top\right) \Big\} \mathbf{t} = \mathbf{b}, \end{aligned} \tag{33}$$

where $\mathbf{b} = \mathbf{p}_k$ or $\mathbf{b} = \mathbf{r}_k$. Let

$$\hat{\mathbf{t}} = \widehat{M}^{-1} \left(\theta_k \widehat{M}_1^\top - \widehat{K}^\top\right) \mathbf{t}, \quad \tilde{\mathbf{t}} = G^{-1} \left(\theta_k F_1^\top - E^\top\right) \mathbf{t},$$

which is equivalent to

$$\left(\widehat{K}^\top - \theta_k \widehat{M}_1^\top\right) \mathbf{t} + \widehat{M}\hat{\mathbf{t}} = 0, \quad \left(E^\top - \theta_k F_1^\top\right) \mathbf{t} + G\tilde{\mathbf{t}} = 0. \tag{34a}$$

Then (33) can be represented as

$$\left(\theta_k K - \theta_k^2 M_1\right) \mathbf{t} + \left(\widehat{K} - \theta_k \widehat{M_1}\right) \hat{\mathbf{t}} + \left(E - \theta_k F_1\right) \tilde{\mathbf{t}} = -\mathbf{b}. \tag{34b}$$

Combining (34a) with (34b), the solution $\mathbf{t}$ in (33) can be solved from the enlarged linear system

$$\begin{bmatrix} \widehat{M} & & \widehat{K}^\top - \theta_k \widehat{M_1}^\top \\ & G & E^\top - \theta_k F_1^\top \\ \widehat{K} - \theta_k \widehat{M_1} & E - \theta_k F_1 & \theta_k K - \theta_k^2 M_1 \end{bmatrix} \begin{bmatrix} \hat{\mathbf{t}} \\ \tilde{\mathbf{t}} \\ \mathbf{t} \end{bmatrix} = \begin{bmatrix} 0 \\ 0 \\ -\mathbf{b} \end{bmatrix}. \tag{35}$$

5.1. Partial locking scheme

To compute successively all other desired eigenvalues, deflation [14, 16] or locking [15, 16, 17, 23] scheme is necessary. The Jacobi-Davidson method incorporated with locking scheme is capable of calculating the smallest positive eigenvalue first and then computing successively all other desired eigenvalues by suitably choosing the orthonormal searching space $\mathrm{span}(V \equiv [V_c, V_0])$, where the columns of V_c form an orthonormal basis of the subspace generated by the convergent eigenvectors and V_0 is any matrix satisfying $V^\top V = I$. Therefore, in each iteration of Algorithm 1, the convergent eigenvalues $\lambda_1, \ldots, \lambda_j$ will be included in the eigenvalues of the projective QEP $(\theta^2 M_2 + \theta M_1 + M_0)\mathbf{s} = 0$ in Line 3 of Algorithm 1. Therefore, we choose the target Ritz value θ in Line 4 of Algorithm 1 with $\theta \notin \{\lambda_1, \ldots, \lambda_j\}$.

Let $\{\lambda_1, \ldots, \lambda_m\}$ be the desired eigenvalues. If m is small, then the locking scheme can be applied to compute successively all desired eigenvalues. However, when m is large, locking all the convergent eigenvectors in the searching subspace $\mathrm{span}(V)$ will reduce the efficiency because it increases the computational costs for computing the eigenpairs of $(\theta^2 M_2 + \theta M_1 + M_0)\mathbf{s} = 0$ and the Ritz vector $\mathbf{u}$, and orthogonalizing correction vector $\mathbf{t}$ against V in Lines 1, 5 and 7, respectively, of Algorithm 1. In order to tackle this drawback, we propose a partial locking scheme with locking ℓ convergent eigenvectors at most in each iteration. That is for computing the $(j+1)$-th eigenpair $(\lambda_{j+1}, \mathbf{x}_{j+1})$ with $j+1 \leq \ell$, all the convergent eigenvectors $\mathbf{x}_1, \ldots, \mathbf{x}_j$ are locked in V which means that the columns of V_c is a orthonormal basis of the subspace $\mathrm{span}\{\mathbf{x}_1, \ldots, \mathbf{x}_j\}$. If $j+1 > \ell$, then only the convergent eigenvectors $\mathbf{x}_{j+1-\ell}, \ldots, \mathbf{x}_j$ are locked. We summarize it in Algorithm 2.

5.2. Partial deflation scheme

In Section 4, an explicit nonequivalence low-rank deflation method is proposed to transform the convergent eigenvalues to infinity, while all other eigenvalues remain unchanged. The next successive eigenvalue thus becomes the smallest positive eigenvalue of the transformed problem. In this subsection, we will discuss how to efficiently apply QJD to solve the deflated QEP $\mathcal{Q}_d(\lambda)\mathbf{x} = 0$ in (27).

Algorithm 2 Quadratic Jacobi-Davidson method with partial locking scheme.

Require: Coefficient matrices A_0, A_1, A_2, number p of desired eigenvalues, locking number ℓ ($\ell < p$) and an initial orthonormal matrix V.

Ensure: The desired eigenpair $(\lambda_j, \mathbf{x}_j)$ for $j = 1, \ldots, p$.

Set $V_c = [\ ]$;
for $j = 1, \ldots, p$ **do**
  Use Algorithm 1 with initial matrix V to compute the desired eigenpair $(\lambda_j, \mathbf{x}_j)$;
  if $j \leq \ell$ **then**
    Orthogonalize $\mathbf{x}_j$ against V_c; set $V_c = [V_c, \mathbf{x}_j/\|\mathbf{x}_j\|_2]$;
  else
    Orthogonalize $\mathbf{x}_j$ against $V_c(:, 2:\ell)$; set $V_c = [V_c(:, 2:\ell), \mathbf{x}_j/\|\mathbf{x}_j\|_2]$;
  end if
  Find an initial matrix V_0 such that $V^\top V = I$ with $V \equiv [V_c, V_0]$.
end for

Let $Y_0 = A_0 X_1 \Lambda_1^{-1} \in \mathbb{R}^{n \times r}$ and $Y_2 = A_2 X_1 \in \mathbb{R}^{n \times r}$. Then the matrices $\widetilde{A}_2$, $\widetilde{A}_1$ and $\widetilde{A}_0$ defined in (28c) can be represented as

$$\widetilde{A}_2 = A_2 - Y_2 \Theta_1 Y_2^\top, \tag{36a}$$

$$\widetilde{A}_1 = A_1 + Y_2 \Theta_1 Y_0^\top + Y_0 \Theta_1 Y_2^\top, \tag{36b}$$

$$\widetilde{A}_0 = A_0 - Y_0 \Theta_1 Y_0^\top. \tag{36c}$$

As stated in (32a), for solving the correction vector $\mathbf{t}_d$, it needs to solve the linear system

$$\left(\theta_k^2 \widetilde{A}_2 + \theta_k \widetilde{A}_1 + \widetilde{A}_0\right) \mathbf{t} = \mathbf{b}. \tag{37}$$

Using (36), (37) can be rewritten as

$$\left[\mathcal{Q}(\theta_k) - (\theta_k Y_2 - Y_0)\, \Theta_1 \left(\theta_k Y_2^\top - Y_0^\top\right)\right] \mathbf{t} = \mathbf{b}. \tag{38}$$

Let

$$U = \theta_k Y_2 - Y_0.$$

Applying the Sherman-Morrison-Woodbury formula, the solution of (38) can be computed as

$$\begin{aligned}
\mathbf{t} &= \left\{\mathcal{Q}(\theta_k) - U \Theta_1 U^\top\right\}^{-1} \mathbf{b} \\
&= \mathcal{Q}(\theta_k)^{-1}\mathbf{b} + \mathcal{Q}(\theta_k)^{-1} U \left(I - \Theta_1 U^\top \mathcal{Q}(\theta_k)^{-1} U\right)^{-1} \Theta_1 U^\top \mathcal{Q}(\theta_k)^{-1}\mathbf{b} \\
&= \mathcal{Q}(\theta_k)^{-1}\mathbf{b} + \mathcal{Q}(\theta_k)^{-1} U \left(\Theta_1^{-1} - U^\top \mathcal{Q}(\theta_k)^{-1} U\right)^{-1} U^\top \mathcal{Q}(\theta_k)^{-1}\mathbf{b}.
\end{aligned}$$

This means that, in each iteration, we need to solve the linear systems

$$\mathcal{Q}(\theta_k) Z = \begin{bmatrix} \tilde{\mathbf{p}}_k & \tilde{\mathbf{r}}_k & U \end{bmatrix}, \tag{39a}$$

where $\tilde{\mathbf{r}}_k = \mathcal{Q}_d(\theta_k)\tilde{\mathbf{u}}_k$ and $\tilde{\mathbf{p}}_k = (2\theta_k\widetilde{A}_2 + \widetilde{A}_1)\tilde{\mathbf{u}}_k$, and compute the correction vector $\mathbf{t}_d$ as

$$\mathbf{t}_d = \eta_k\tilde{\mathbf{t}}_1 - \tilde{\mathbf{t}}_2 \quad \text{with} \quad \eta_k = \frac{\tilde{\mathbf{u}}_k^*\tilde{\mathbf{t}}_2}{\tilde{\mathbf{u}}_k^*\tilde{\mathbf{t}}_1} \tag{39b}$$

where

$$\tilde{\mathbf{t}}_1 = Z(:,1) + Z(:,3:r+2)(\Theta_1^{-1} - U^\top Z(:,3:r+2))^{-1}U^\top Z(:,1), \tag{39c}$$

$$\tilde{\mathbf{t}}_2 = Z(:,2) + Z(:,3:r+2)(\Theta_1^{-1} - U^\top Z(:,3:r+2))^{-1}U^\top Z(:,2). \tag{39d}$$

From above, we can see that the computational cost of solving $\mathcal{Q}_d(\lambda)\mathbf{x} = 0$ by QJD will be increasing as r is increasing. In order to reduce the computational cost, similar to the concept of partial locking scheme, we propose a partial deflation scheme with deflating ℓ convergent eigenvectors at most in each iteration. That is for computing the $(j+1)$-th eigenpair $(\lambda_{j+1}, \mathbf{x}_{j+1})$ with $j+1 \leq \ell$, all the convergent eigenvectors $\mathbf{x}_1, \ldots, \mathbf{x}_j$ are deflated. If $j+1 > \ell$, then only the convergent eigenvectors $\mathbf{x}_{j+1-\ell}, \ldots, \mathbf{x}_j$ are deflated. We summarize it in Algorithm 3.

Algorithm 3 Quadratic Jacobi-Davidson method with partial deflation scheme.

Require: Coefficient matrices A_0, A_1, A_2, number p of desired eigenvalues, number ℓ ($\ell < p$) of deflation and an initial orthonormal matrix V.
Ensure: The desired eigenpair $(\lambda_j, \mathbf{x}_j)$ for $j = 1, \ldots, p$.

Set $X_1 = [\ ]$, $Y_0 = [\ ]$, $Y_2 = [\ ]$ and $\Theta = [\ ]$;
for $j = 1, \ldots, p$ **do**
  Use Algorithm 1 with initial matrix V and solving correction vector $\mathbf{t}_d$ by (39) to compute the first desired eigenpair $(\lambda_j, \mathbf{x}_j)$ of $\mathcal{Q}_d(\lambda)\mathbf{x} = 0$;
  Compute $\mathbf{y}_0 = \lambda_j^{-1}A_0\mathbf{x}_j$ and $\mathbf{y}_2 = A_2\mathbf{x}_j$;
  if $j \leq \ell$ **then**
    Set $\Theta = \begin{bmatrix} \Theta & X_1^\top\mathbf{y}_2 \\ \mathbf{x}_j^\top Y_2 & \mathbf{x}_j^\top\mathbf{y}_2 \end{bmatrix}$, $\Theta_1 = \Theta^{-1}$, $X_1 = [X_1, \mathbf{x}_j]$, $Y_0 = [Y_0, \mathbf{y}_0]$ and $Y_2 = [Y_2, \mathbf{y}_2]$;
  else
    Set $\Theta = \begin{bmatrix} \Theta(2:\ell, 2:\ell) & X_1(:,2:\ell)^\top\mathbf{y}_2 \\ \mathbf{x}_j^\top Y_2(:,2:\ell) & \mathbf{x}_j^\top\mathbf{y}_2 \end{bmatrix}$ and $\Theta_1 = \Theta^{-1}$;
    Set $X_1 = [X_1(:,2:\ell), \mathbf{x}_j]$, $Y_0 = [Y_0(:,2:\ell), \mathbf{y}_0]$ and $Y_2 = [Y_2(:,2:\ell), \mathbf{y}_2]$;
  end if
  Update the initial matrix V.
end for

6. Numerical results

In what follows, we will compare that the efficiency and robustness of Algorithm 2 with $\ell = 20$ and Algorithm 3 with $\ell = 10$ for computing desired

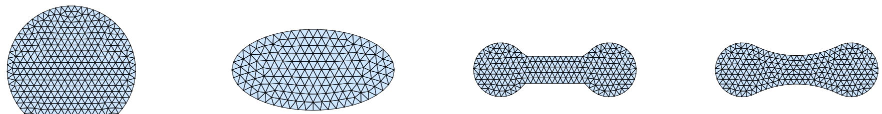

(a) Disk (b) Ellipse (c) Dumbbell (d) Peanut

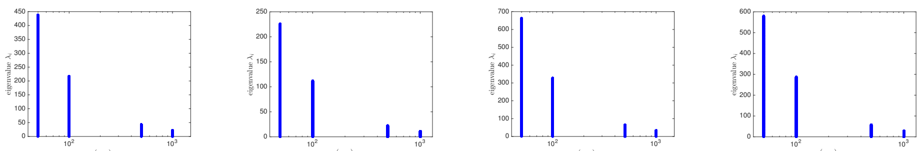

(e) λ_i for disk (f) λ_i for ellipse (g) λ_i for dumbbell (h) λ_i for peanut

Figure 1: Model domains and the associated distributions of the 5000 positive target eigenvalues for $\varepsilon(x, y) = 50, 100, 500, 1000$.

Table 2: The matrix dimension n, m ($K \in \mathbb{R}^{n\times n}$, $E \in \mathbb{R}^{n\times m}$) of the matrices for the benchmark problems.

Domain	disk	ellipse	dumbbell	peanut
(n, m)	(124631, 1150)	(71546, 976)	(149047, 1871)	(168548, 1492)

positive real transmission eigenvalues $\lambda_i > 0$, $i = 1, \ldots, p$, on four different domains [22] as shown in Figure 1. The tetrahedra mesh is used to construct the meshes for these domains. The associated matrix dimensions n and m of the matrices in Table 1 are listed in Table 2. The distributions of $\{\lambda_1, \ldots, \lambda_p\}$ with $\varepsilon(x, y) = 50, 100, 500, 1000$ and matrix dimensions n and m in Table 2 are shown in Figures 1(e), 1(f), 1(g) and 1(h), respectively. All the eigenvalues almost have an uniform distribution.

All computations in this section are carried out in MATLAB 2015b. The system in (35) is solved by the direct method. For the hardware configuration, we use an HP server that is equipped with two Intel Quad-Core Xeon E5-2643 3.33 GHz CPUs, 96 GB of main memory, and the RedHat Linux operating system.

6.1. Numerical validation for the clustering eigenvalues

In this section, we shall numerically validate that the TEP has a dense spectrum in the interval $(0, O(1))$ if the coefficient $\varepsilon(x, y)$ in (1a) is sufficient large as shown in Remark 3. Furthermore, we shall demonstrate that each eigencurve can be numerically approximated by a nonlinear function.

In order to observe the variety of the distribution of the eigenvalues with changing the coefficient $\varepsilon(x, y)$, we compute the fifty smallest positive real eigenvalues for each given constant $\varepsilon(x, y) = \varepsilon_0$ and show the computed eigenvalues in Figures 2(a), 2(c), 2(e) and 2(g). From these results, we see that the distribu-

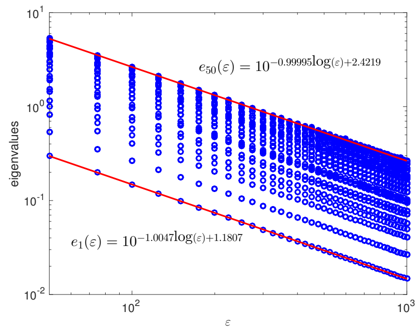

(a) Eigenvalues for disk

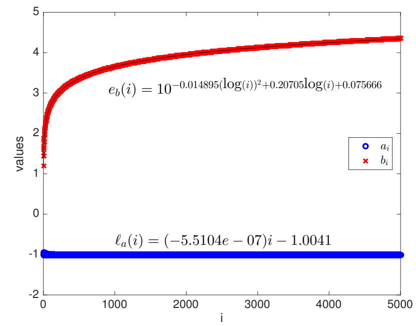

(b) Coefficients a_i and b_i for disk

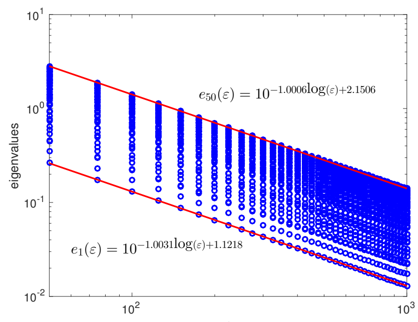

(c) Eigenvalues for ellipse

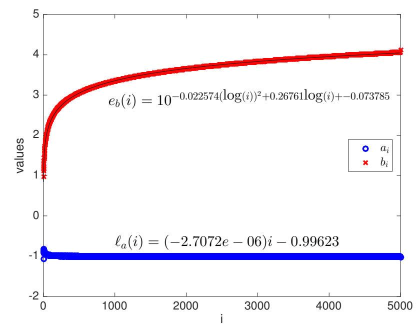

(d) Coefficients a_i and b_i for ellipse

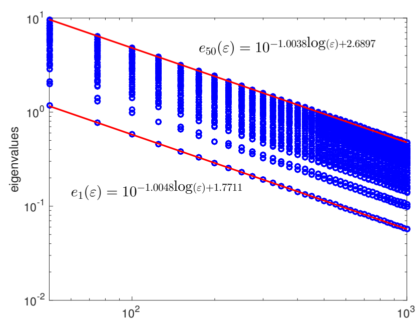

(e) Eigenvalues for dumbbell

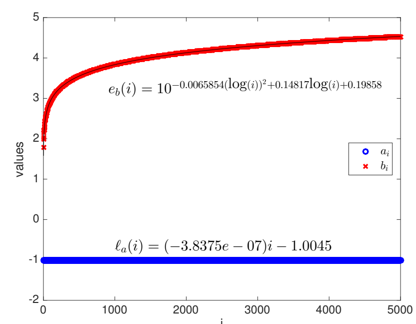

(f) Coefficients a_i and b_i for dumbbell

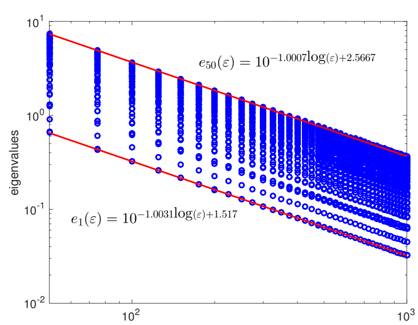

(g) Eigenvalues for peanut

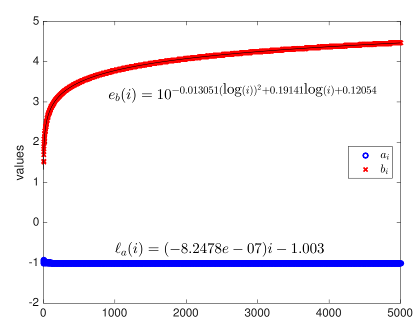

(h) Coefficients a_i and b_i for peanut

Figure 2: Eigenvalues with various $\varepsilon(x, y)$ and the coefficients a_i and b_i in the nonlinear functions.

Table 3: The first and pth eigenvalues λ_1 and λ_p computed by Algorithm 3 and the associated $(e_1(\varepsilon_0), e_p(\varepsilon_0))$ defined in (40), where $p = 5000$ and $\varepsilon_0 = 5000$.

Domain	disk	ellipse
$(e_1(\varepsilon_0), e_p(\varepsilon_0))$	$(0.00290, 4.25)$	$(1.837 \times 10^{-3}, 2.129)$
(λ_1, λ_p)	$(0.00294, 4.28)$	$(2.087 \times 10^{-3}, 2.210)$
(r_1, r_p)	$(0.014, 0.007)$	$(0.119, 0.037)$
Domain	dumbbell	peanut
$(e_1(\varepsilon_0), e_p(\varepsilon_0))$	$(0.0113, 6.42)$	$(6.392 \times 10^{-3}, 5.621)$
(λ_1, λ_p)	$(0.0114, 6.49)$	$(6.440 \times 10^{-3}, 5.673)$
(r_1, r_p)	$(0.009, 0.011)$	$(0.007, 0.009)$

tions of these fifty eigenvalues is clustered to the interval (0.2,1) as ε_0 approaches to 10^3.

On the other hand, these results also show that each eigencurve $\lambda_i(\varepsilon_0)$ can be approximated by a nonlinear function

$$\lambda_i(\varepsilon_0) \approx e_i(\varepsilon_0) \equiv 10^{a_i \log_{10}(\varepsilon_0) + b_i} \tag{40}$$

with constant a_i and b_i for $i = 1, \ldots, 50$. We show the nonlinear functions $e_1(\varepsilon)$ and $e_{50}(\varepsilon)$ in Figures 2(a), 2(c), 2(e) and 2(g) with red lines. These approximations can be extended to other eigencurves. Using the eigenvalues shown in Figures 1(e), 1(f), 1(g) and 1(h), we get the coefficients a_i and b_i for $i = 1, \ldots, 5000$ as shown in Figures 2(b), 2(d), 2(f) and 2(h), respectively. The approximation in (40) can be used to estimate the eigenvalues for a given ε_0. In Table 3, we demonstrate the computed eigenvalues λ_1 and λ_p by Algorithm 3 and $(e_1(\varepsilon_0), e_p(\varepsilon_0))$ in (40) for $\varepsilon_0 = 5000$ and $p = 5000$ with the domains in Figure 1. The results show that the relative errors $r_i \equiv |\lambda_i - e_i|/|\lambda_i|$ can be achieved about 0.01 for $i = 1$ and p.

Furthermore, the curves of the coefficients a_i and b_i for $i = 1, \ldots, 5000$ in Figures 2(b), 2(d), 2(f) and 2(h) can be approximated by a linear function

$$a_i \approx \ell_a(i) \equiv \alpha_1 \times i + \alpha_0 \tag{41a}$$

and a nonlinear function

$$b_i \approx e_b(i) \equiv 10^{\beta_2 (\log_{10}(i))^2 + \beta_1 \log_{10}(i) + \beta_0}, \tag{41b}$$

respectively, as shown in the associated figures. Substituting (41) into (40), we can see that the positive eigencurve $\lambda_i(\varepsilon)$ can be approximated by

$$\lambda_i(\varepsilon) \approx e(\varepsilon, i) \equiv 10^{(\alpha_1 \times i + \alpha_0) \log_{10}(\varepsilon) + 10^{\beta_2 (\log_{10}(i))^2 + \beta_1 \log_{10}(i) + \beta_0}}.$$

Comparing with the eigenvalues $\lambda_i(100)$, for $i = 5001, \ldots, 10105$, of the TEP with peanut domain as shown in Figure 5(b), the relative residuals $|\lambda_i(100) - e(100, i)|/\lambda_i(100)$ for $i = 5001, \ldots, 10105$ range from 0.01 to 0.07. This demonstrates that $e(\varepsilon, i)$ is a good approximation for the eigencurve.

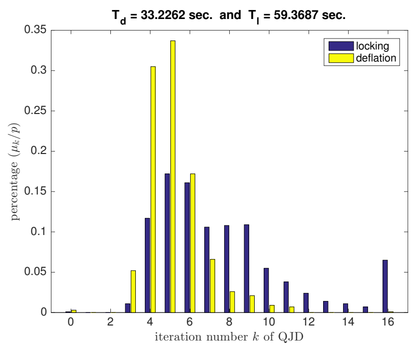

(a) Ellipse with $\varepsilon_0 = 50$ and $p = 1000$

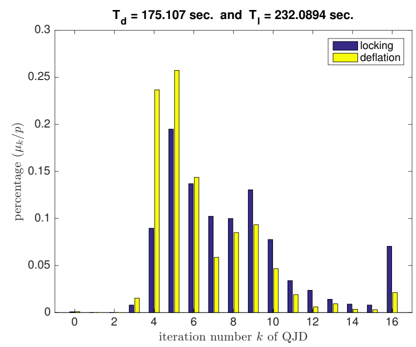

(b) Peanut with $\varepsilon_0 = 100$ and $p = 3000$

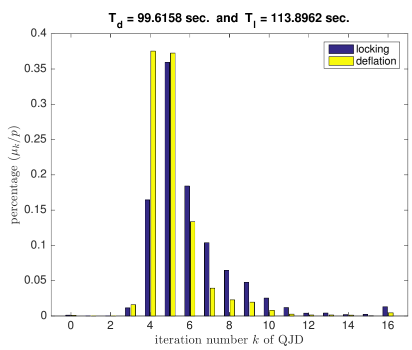

(c) Dumbbell with $\varepsilon_0 = 500$ and $p = 5000$

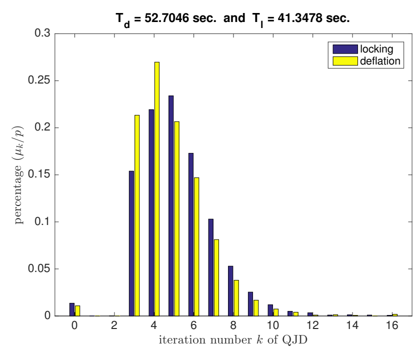

(d) Disk with $\varepsilon_0 = 1000$ and $p = 5000$

Figure 3: Percentages $\frac{\mu_k}{p}$ for the locking scheme and the deflation scheme with various ε_0.

6.2. Numerical comparison for locking and deflation schemes

Let μ_k denote the number of the target eigenvalues which are computed by QJD in Algorithm 1 with using k iterations. If $k \geq 16$, then we define $\mu_{16} := \sum_{k\geq 16} \mu_k$. On the other hand, we define T_l and T_d to be the average of the CPU times for computing p target positive smallest eigenvalues by Algorithms 2 and 3, respectively.

In Figure 3, we show the percentage μ_k/p for $k = 0, 1, \ldots, 16$ with $\varepsilon_0 = 50, 100, 500, 1000$. The results demonstrate that the iteration numbers k of Algorithm 3 with deflation scheme are concentrated at $k = 4, 5, 6$ for each ε_0. However, the iteration number k of Algorithm 2 with locking scheme is depend on ε_0. The iteration number is concentrated at $4, 5, 6$ only when ε_0 is large enough as shown in Figures 3(c) and 3(d). Figures 3(a) and 3(b) show that, in average, locking scheme will be needed more and more iterations to compute the target eigenpair as ε_0 to be small. When the convergent eigenvectors are locked into the searching subspace span$\{V\}$, the small size QEP $(\theta^2 M_2 + \theta M_1 + M_0)\mathbf{s} = 0$ in Line 3 at Algorithm 1 will produce dummy ritz pairs. The convergence of the locking scheme can be affected by such dummy ritz pairs when the distribution of the eigenvalues is not clustered such as $\varepsilon_0 = 50, 100$. In the deflation scheme, there is no any dummy ritz pairs produced by the convergent eigenvectors. This is a reason why, in average, the iteration number for the deflation scheme is less than that for the locking scheme. This means that the deflation scheme is more robust than the locking scheme for ε_0.

From Section 5, we know that the computational cost of the deflation scheme is more than that of the locking scheme in each iteration. As shown in Figures 3(a), 3(b) and 3(c), due to the total iteration numbers of deflation scheme to be obviously less than that of locking scheme for $\varepsilon_0 = 50$, 100 and 500, the average time T_d is less than T_l. For $\varepsilon_0 = 1000$, both the iteration numbers of the locking and deflation schemes are concentrated at $3, 4, 5, 6$. This leads to $T_d > T_l$ as shown in Figure 3(d).

In order to demonstrate the robustness of Algorithm 3, we compute the first 5000 eigenpairs of the TEP with domains in Figure 1 by Algorithm 3. The percentages $\frac{\mu_k}{p}$ with $\varepsilon_0 = 50, 100, 500, 1000$ are shown in Figure 4. The results tell us that only at $\varepsilon_0 = 50$, more iteration numbers of the QJD are needed to compute the target eigenvalues. The most iterations of the QJD are concentrated at $3, 4, 5, 6$ for other ε_0.

6.3. Computing the eigenvalues in the given interval

In Subsection 6.2, we have demonstrated that Algorithms 2 and 3 can be applied to sequently compute a lot of the target eigenpairs. Even each target eigenvalue can be efficiently computed by the proposed methods, the total CPU times are huge when the number of target eigenvalues is huge. In order to reduce the total CPU times, we slightly modify Algorithm 3 so that it can be applied to compute the eigenvalues in a given interval. We called it as Mod. Alg. 3. Therefore, the target eigenvalues can be computed by Mod. Alg. 3 in parallel with a given different interval. In Figure 5, we show the results of the domain

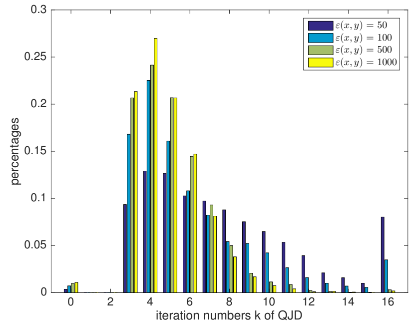

(a) Disk

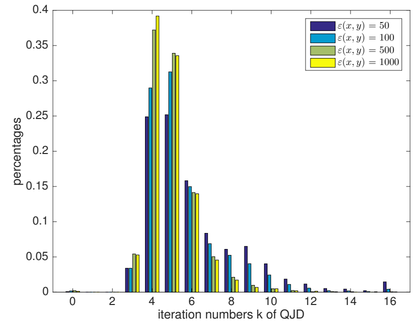

(b) Ellipse

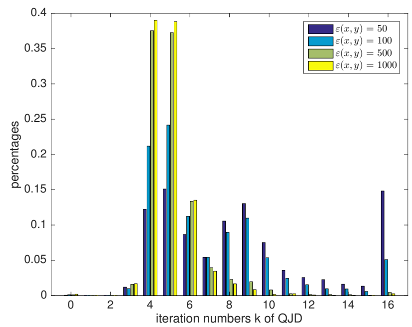

(c) Dumbbell

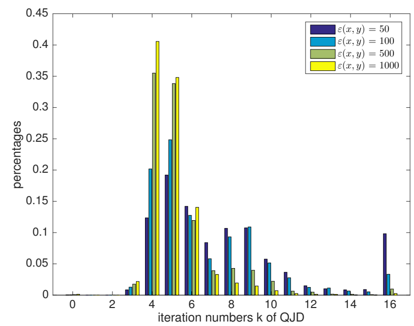

(d) Peanut

Figure 4: Percentage $\frac{\mu_k}{p}$ for the deflation scheme with various ε_0.

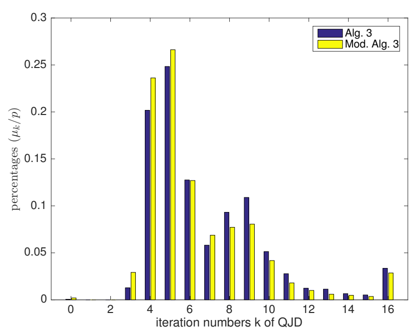

(a) Percentage $\frac{\mu_k}{p}$ for $\lambda_1, \ldots, \lambda_{5000}$

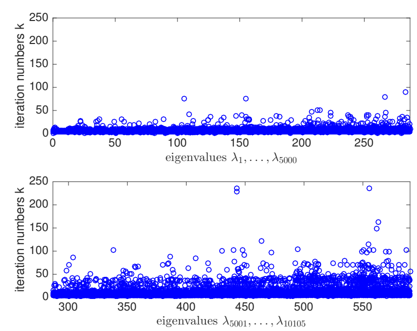

(b) Iteration numbers k of QJD for computing λ_i, $i = 1, \ldots, 10105$

Figure 5: Peanut with $\varepsilon(x, y) = 100$.

peanut with $\varepsilon_0 = 100$ and the given intervals $(10i, 10(i+1)]$ for $i = 0, 1, \ldots, 59$. That is we apply Mod. Alg. 3 to compute all eigenvalues in the interval $(0, 600]$.

Compared the percentage $\frac{\mu_k}{5000}$ in computing $\lambda_1, \ldots, \lambda_{5000}$ with Algorithm 3 and Mod. Alg. 3, the results in Figure 5(a) show that the percentage $\frac{\mu_3+\cdots+\mu_7}{5000}$ for Algorithm 3 and Mod. Alg. 3 are equal to 0.6488 and 0.7274, respectively. This means that, in average, the convergence of Mod. Alg. 3 is better than that of Algorithm 3. On the other hand, in Figure 5(b), we demonstrate the iteration numbers of the QJD in Mod. Alg. 3 for computing each eigenvalues. These results show that it needs more and more iteration numbers of the QJD as the target eigenvalue is larger and larger.

7. Conclusion

In this paper, we consider the Maxwell's equation with complex media in pseudo-chiral model and the transverse magnetic mode to derive the two-dimensional transmission eigenvalue problem in (1) with $\varepsilon(x, y) = n(x, y) + \gamma^2$, where $n(x, y)$ is the index of refraction and $\gamma > 0$ is a chirality parameter. The associated discretized eigenvalue problem is related to a generalized eigenvalue problem which can be reduced to a quadratic eigenvalue problem (QEP) by deflating all nonphysical zeros. We estimate half of the positive eigenvalues of the QEP are on some interval which forms a dense spectrum of the QEP. The quadratic Jacobi-Davidson (QJD) method with partial locking technique is proposed to compute the dense spectrum of the QEP. In order to accelerate convergence, we also develop a so-called non-equivalence deflation technique combined with QJD to deflate the part of computed eigenvalues to infinity while keeping the other eigenvalues unchanged. Numerical results demonstrate that the deflation technique makes the convergence efficiently and robustly. The locking technique outperforms the deflation technique in timing only when eigenvalues of the QEP are typically clustering together in our model. Numerical results also illustrate that the eigenvalue curves can be approximated by the nonlinear functions so that we can apply these nonlinear functions to estimate the eigenvalues for a given constant $\varepsilon(x, y)$.

Acknowledgments

The first author's work was partially supported by the Ministry of Science and Technology (MoST), National Center of Theoretical Sciences (NCTS) in Taiwan. The third author's work was partially supported by MoST, NCTS and ST Yau Center in Taiwan.

References

[1] F. Cakoni, D. Colton, P. Monk, and J. Sun. The inverse electromagnetic scattering problem for anisotropic media. *Inv. Prob.*, 26(7):074004, 2010.

[2] F. Cakoni, D. Gintides, and H. Haddar. The existence of an infinite discrete set of transmission eigenvalues. *SIAM J. Math. Anal.*, 42(1):237–255, 2010.

[3] F. Cakoni and H. Haddar. On the existence of transmission eigenvalues in an inhomogeneous medium. *Appl. Anal.*, 88(4):475–493, 2009.

[4] F. Cakoni and H. Haddar. Transmission eigenvalues in inverse scattering theory. In G. Uhlmann, editor, *Inverse Problems and Applications: Inside Out II*, volume 60 of *Math. Sci. Res. Inst. Publ.*, pages 527–578. Cambridge University Press, Cambridge, 2012.

[5] Q. Chen, H. Haddar, A. Lechtleiter, and P. Monk. A sampling method for inverse scattering in the time domain. *Inv. Prob.*, 26:085001, 2010.

[6] D. Colton, J. Coyle, and P. Monk. Recent developments in inverse acoustic scattering theory. *SIAM Rev.*, 42:369–414, 2000.

[7] D. Colton and H. Haddar. An application of the reciprocity gap functional to inverse scattering theory. *Inv. Prob.*, 21:383–98, 2005.

[8] D. Colton and R. Kress. *Inverse Acoustic and Electromagnetic Scattering Theory*, volume 93 of *Applied Mathematical Sciences*. Springer, New York, 3rd edition, 2013.

[9] D. Colton and P. Monk. A novel method for solving the inverse scattering problem for time-harmonic acoustic waves in the resonance region. *SIAM J. Appl. Math.*, 45:1039–53, 1985.

[10] D. Colton, P. Monk, and J. Sun. Analytical and computational methods for transmission eigenvalues. *Inv. Prob.*, 26:045011, 2010.

[11] D. Colton, L. Päivärinta, and J. Sylvester. The interior transmission problem. *Inv. Prob. Imaging*, 1(1):13–28, 2007.

[12] G. C. Hsiao, F. Liu, J. Sun, and L. Xu. A coupled BEM and FEM for the interior transmission problem in acoustics. *J. Comput. Appl. Math.*, 235:5213–5221, 2011.

[13] T.-M. Huang, W.-Q. Huang, and W.-W. Lin. A robust numerical algorithm for computing Maxwell's transmission eigenvalue problems. *SIAM J. Sci. Comput.*, 37:A2403–A2423, 2015.

[14] T.-M. Huang and W.-W. Lin. A novel deflation technique for solving quadratice eigenvalue problems. *Bulletin of the Institute of Mathematics, Academia Sinica (New Series)*, 9:57–84, 2014.

[15] T.-M. Huang, W. Wang, and C.-T. Lee. An efficiency study of polynomial eigenvalue problem solvers for quantum dot simulations. *Taiwanese J. Math.*, 14:999–1021, 2010.

[16] T.-M. Hwang, W.-W. Lin, J.-L. Liu, and W. Wang. Jacobi-Davidson methods for cubic eigenvalue problems. *Numer. Linear Algebra Appl.*, 12:605–624, 2005.

[17] T.-M. Hwang, W.-W. Lin, W.-C. Wang, and W. Wang. Numerical simulation of three dimensional pyramid quantum dot. *J. Comput. Phys.*, 196:208–232, 2004.

[18] X. Ji, J. Sun, and T. Turner. Algorithm 922: A mixed finite element method for Helmholtz transmission eigenvalues. *ACM Trans. Math. Software*, 38:29, 2012.

[19] X. Ji, J. Sun, and H. Xie. A multigrid method for Helmholtz transmission eigenvalue problems. *J. Sci. Comput.*, 60(2):276–294, 2014.

[20] A. Kirsch. On the existence of transmission eigenvalues. *Inv. Prob. Imaging*, 3(2):155–172, 2009.

[21] A. Kleefeld. A numerical method to compute interior transmission eigenvalues. *Inv. Prob.*, 29(10):104012, 2013.

[22] T. Li, W.-Q. Huang, W.-W. Lin, and J. Liu. On spectral analysis and a novel algorithm for transmission eigenvalue problems. *J. Sci. Comput.*, 64(1):83–108, 2015.

[23] K. Meerbergen. Locking and restarting quadratic eigenvalue solvers. *SIAM J. Sci. Comput.*, 22:1814–1839, 2001.

[24] P. Monk and J. Sun. Inverse scattering using finite elements and gap reciprocity. *Inv. Prob. Imaging*, 1:643–60, 2007.

[25] P. Monk and J. Sun. Finite element methods for Maxwell's transmission eigenvalues. *SIAM J. Sci. Comput.*, 34:B247–B264, 2012.

[26] L. Päivärinta and J. Sylvester. Transmission eigenvalues. *SIAM J. Math. Anal.*, 40(2):738–753, 2008.

[27] A. Serdyukov, I. Semchenko, S. Tretyakov, and A. Sihvola. *Electromagnetics of Bi-anisotropic Materials: Theory and Applications*. Gordon and Breach Science, 2001.

[28] G. L. G. Sleijpen, A. G. L. Booten, D. R. Fokkema, and H. A. van der Vorst. Jacobi-Davidson type methods for generalized eigenproblems and polynomial eigenproblems. *BIT*, 36:595–633, 1996.

[29] J. Sun. Iterative methods for transmission eigenvalues. *SIAM J. Numer. Anal.*, 49(5):1860–1874, 2011.

[30] J. Sun. An eigenvalue method using multiple frequency data for inverse scattering problems. *Inv. Prob.*, 28:025012, 2012.

[31] J. Sun and L. Xu. Computation of Maxwell's transmission eigenvalues and its applications in inverse medium problems. *Inv. Prob.*, 29:104013, 2013.

[32] W. S. Weiglhofer and A. Lakhtakia. *Introduction to Complex Mediums for Optics and Electromagnetics*. SPIE, Washington, DC, 2003.